Geomechanics and Engineering, *Vol. 30, No. 6 (2022) 525-538*
https://doi.org/10.12989/gae.2022.30.6.525

A comparative study between the new model and the current model for T-shaped combined footings

Jesús Rafael Garay-Gallegos[a], Arnulfo Luévanos-Rojas*, Sandra López-Chavarría[b], Manuel Medina-Elizondo[c], Gabriel Aguilera-Mancilla[d] and Edith García-Canales[e]

Institute of Multidisciplinary Researches, Autonomous University of Coahuila, Blvd. Revolución No, 151 Ote, CP 27000, Torreón, Coahuila, México

(*Received September 20, 2019, Revised June 9, 2022, Accepted August 27, 2022*)

Abstract. This paper presents a more general model for T-shaped combined footings that support two columns aligned on a longitudinal axis and each column provides an axial load and two orthogonal moments. This model can be applied to the following conditions: (1) without restrictions on its sides, (2) a restricted side and (3) two opposite sides restricted. This model considers the linear soil pressure. The recently published works have been developed for a restricted side and for two opposite sides restricted by Luévanos-Rojas *et al.* (2018a, b). The current model considers the uniform pressure distribution because the position of the resultant force coincides with the center of gravity of the surface of the footing in contact with the soil in direction of the longitudinal axis where the columns are located. This paper shows three numerical examples. Example 1 is for a T-shaped combined footing with a limited side (one column is located on the property boundary). Example 2 is for a T-shaped combined footing with two limited opposite sides (the two columns are located on the property boundary). Example 3 is for a T-shaped combined footing with two limited opposite sides, one column is located in the center of the width of the upper flange ($b_1/2=L_1$), and other column is located at a distance half the width of the strip from the free end of the footing ($b_2/2=b-L_1-L$). The main advantage of this work over other works is that this model can be applied to T-shaped combined footings without restrictions on its sides, a restricted side and two opposite sides restricted. It also shows the deficiencies of the current model over the new model.

Keywords: bending moments; bending shear; combined footings; punching shear; reinforced concrete

1. Introduction

1.1 Background

The soil pressure under a footing depends on the type of soil, the relative stiffness of the soil and the footing, and the depth of the foundation at the level of contact between the footing and the soil.

Fig. 1 shows the distribution of soil pressure under a footing according to the type of soil and the stiffness of the footing. Fig. 1(a) presents a rigid footing on sandy soil. Fig. 1(b) shows a rigid footing on clay soil. Fig. 1(c) presents a flexible footing on sandy soil. Fig. 1(d) shows a flexible footing on clay soil. Fig. 1(e) presents the uniform distribution used in the current design (Bowles, 2001).

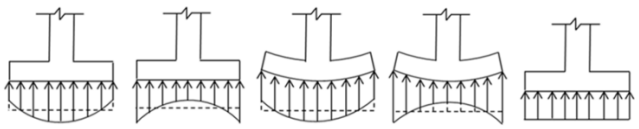

(a) (b) (c) (d) (e)

Fig. 1 Distribution of the soil pressure under of the footing

The pressure distribution diagrams (Fig. 1) can be applied when the center of gravity of the footing coincides with the position of the resultant force.

The current model considers the uniform pressure distribution because the position of the resultant force coincides with the center of gravity of the surface of the footing in contact with the soil in direction of the longitudinal axis where the columns are located.

The new model considers the linear pressure distribution for design of T-shaped combined footings subject to an axial load and two orthogonal bending moments in each column.

This work presents the equations of the bending moments, bending shear and punching shear for a linear pressure distribution (new model) and for a uniform pressure distribution (current model).

*Corresponding author, Ph.D.
E-mail: arnulfol_2007@hotmail.com
[a]Ph.D. Candidate
E-mail: drgaray24@hotmail.com
[b]Ph.D.
E-mail: sandylopez5@hotmail.com
[c]Ph.D.
E-mail: drmanuelmedina@yahoo.com.mx
[d]Ph.D.
E-mail: gabo76mancilla@hotmail.com
[e]Ph.D. Candidate
E-mail: gc_edith@hotmail.com

ISSN: 2005-307X (Print), 2092-6219 (Online)

1.2 Literature review

The main studies of several researchers on foundation structures and mathematical models for footings have been investigated successfully in several geotechnical engineering problems in the last decade are: Chen *et al*. (2011) established the nonlinear partial differential equations of motion for hybrid composite plates under to initial stresses on elastic foundations to study the non-linear vibration behavior. Shahin and Cheung (2011) proposed stochastic design graphs for the load capacity of the strip footings. Zhang *et al.* (2011) presented a non-linear analysis of finite beams supported by winkler taking into account the resistance effect of the beam-soil interface. Agrawal and Hora (2012) presented a document as a single integral compatible structural (building frame, walls, columns, isolated footings, and soil mass) to predict the nonlinear interaction behaviour of the composite system under seismic loads. Rad (2012) used the state-space and differential quadrature methods to study the static behavior of a bi-directional circular plate of functionally graded non-uniform thickness resting on quadratically gradient elastic foundations (Winkler-Pasternak type) subjected to transverse shear loads and in plane symmetrical. Maheshwari and Khatri (2012) investigated the influence of the inclusion of geosynthetic layer on the response of combined footings on reinforced ground beds with stone columns. Orbanich *et al.* (2012) realized a study on strenghtening and repair of concrete foundation beams with carbon fiber composite materials and the numerical model is performed by the Finite Elements Method with the Abaqus program. Mohamed *et al*. (2013) adjusted the Schmertmann's equation to estimate the settlement of the shallow footings supported on unsaturated and saturated sandy soils. Luévanos-Rojas *et al.* (2013) developed a mathematical model for the design of reinforced concrete rectangular isolated footings taking into account the linear pressure of the soil. Orbanich and Ortega (2013) developed a numeric procedure to analyse the elastic foundation plates with internal and perimetric stiffening beams on elastic foundations by means of the Finite Differences Method considering the stiffness of the plate, the perimetric and internal plate beams and the soil reaction module. Dixit and Patil (2013) experimentally evaluated the bearing capacity factor Nγ and corresponding settlements for square footings in a finite layer of sand, and it was compared with the Nγ values of Terzaghi, Meyerhof, Hansen and Vesic's. ErzÍn and Gul (2013) used the neural networks to predict the settlement of pad footings on non-cohesive soils based on a standard penetration test. Cure *et al*. (2014) carried out a series of load capacity tests with the eccentrically loaded model surface and shallow strip footings supported near to a slope to study the behaviour of these footings (ultimate loads, failure surfaces, load-displacement curves, rotation of footing, etc.). Luévanos-Rojas (2014a) designed a model for the reinforced concrete circular isolated footings taking into account the linear pressure of the soil. Luévanos-Rojas (2014b) developed a model for the design of reinforced concrete rectangular combined footings with a property line taking into account the linear pressure of the soil. Uncuoğlu (2015) investigated numerically by mean a series of three-dimensional non-linear finite element analyses to determine the ultimate bearing capacity and failure mechanism of square footings resting on a sand layer over clay. Luévanos-Rojas (2015) designed a model for the reinforced concrete trapezoidal combined footings with a property line taking into account the linear pressure of the soil. Luévanos-Rojas (2016a) realized a comparative study for the design of reinforced concrete rectangular and circular isolated footings. Luévanos-Rojas (2016b) developed a model for the design of reinforced concrete rectangular combined footings with two property lines restricted (opposite sides) taking into account the linear pressure of the soil. Anil *et al.* (2017) experimentally and analytically investigated the load capacities and settlement profiles of six irregularly shaped footings located on sand subjected to the effect of axial load. López-Chavarría *et al.* (2017) developed a general model for the design of reinforced concrete square isolated footings taking into account the linear pressure of the soil. Khatri *et al.* (2017) presented a laboratory experimental study of the pressure-settlement behavior of square and rectangular skirted footing supported on sand and subjected to a vertical load. Luévanos-Rojas *et al.* (2017) realized a comparative study for the design of reinforced concrete trapezoidal and rectangular isolated footings. Mohebkhah (2017) presented a two-dimensional numerical model by mean the discrete element method to obtain the ultimate load capacity of a strip footing on soft clay reinforced with a stone masonry trench. Luévanos-Rojas *et al.* (2018b) developed a mathematical model for design of reinforced concrete T-shaped combined footings. Alijani and Bidgoli (2018) analyzed the vibration of a reinforced concrete foundation by SiO_2 nanoparticles supported on soil bed. Dezhkam and Yaghfoori (2018) studied the vibration of concrete foundations supported on soil medium, the soil medium is simulated by Winkler model, and the concrete foundation is modeled by thick plate elements based on classical plate theory. Bensaid and Kerboua (2019) investigated the thermal stability characteristics of carbon nanotube reinforced composite beams on elastic foundation and subjected to increasing loads and external uniform temperature. Yáñez-Palafox *et al.* (2019) presented a mathematical model for design of the strap combined footings. Turedi *et al.* (2019) numerically analyzed and laboratory tests the load settlement and vertical stress of the ring footings on the loose sand bed.

The works related to this paper are: Luévanos-Rojas *et al.* (2018a) proposed a mathematical model to obtain the minimum surface in contact with the soil of the reinforced concrete T-shaped combined footings. Luévanos-Rojas *et al.* (2018b) developed a mathematical model to obtain the effective depth and reinforcing steel for design of reinforced concrete T-shaped combined footings. These two models consider a limited side on the property line and two limited opposite sides on the property line, but these do not take into account the case without restrictions on its opposite sides. These also do not show the comparison between the models proposed by Luévanos-Rojas *et al.* (2018a, b) and the current model for design. The current model considers the uniform pressure distribution on the longitudinal axis,

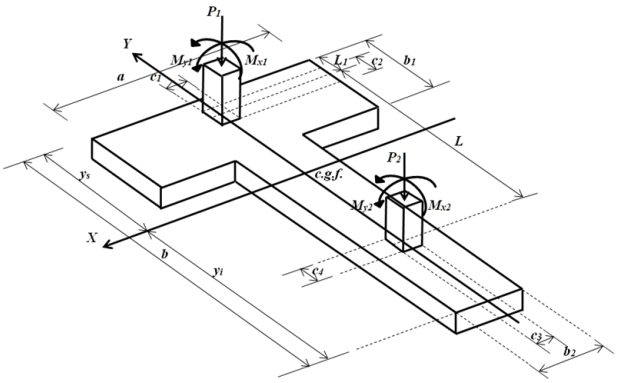

Fig. 2 T-shaped combined footing with unrestricted sides

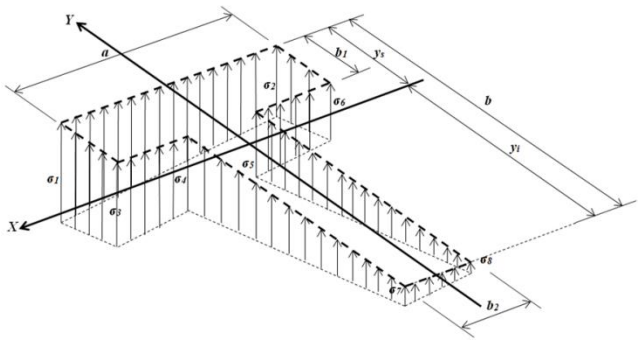

Fig. 3 Diagram of pressure on the T-shaped combined footing with unrestricted sides

where the columns are located.

Thus, the review of the previous studies shows that there is no relationship with the topic of the mathematical model for the design of T-shaped combined footings that is shown in this work.

1.3 Research objective

This work shows a more general model (without restrictions on its sides, a limited side (one column is located on the property boundary) and two limited opposite sides (the two columns are located on the property boundary) for the design of T-shaped combined footings that support two columns aligned on a longitudinal axis subjected to an axial load and two orthogonal moments in each column, and also the distribution of the soil pressure under of the footing is considered linear. The recently published works are restricted for a limited side and for two limited opposite sides. The current model considers the uniform pressure distribution because the position of the resultant force of the axial loads and moments is made to coincide with the center of gravity of the surface of the footing in contact with the soil in direction of the longitudinal axis where the columns are located. Also, three numerical examples are shown to obtain the design of T-shaped combined footings subjected to an axial load and two moments in orthogonal directions in each column by the proposed model and the current model. First example is for a limited side by a property line. Second example is for two limited opposite sides by two property lines. Third example is with two limited opposite sides, one column is located in the center of the width of the upper flange ($b_1/2=L_1$), and other column is located at a distance half the width of the strip from the free end of the footing ($b_2/2=b–L_1–L$).

2. Methodology

The considerations of this work are: the footing is rigid and the soil that supports to the footing is elastic and homogeneous, that comply with the biaxial bending, i.e., the variation of soil pressure is linear.

Fig. 2 shows a T-shaped combined footing with unrestricted sides that supports two columns aligned on a longitudinal axis (Y axis), and each column provides an axial load and two orthogonal bending moments.

Fig. 3 presents the pressure diagram below of the T-shaped combined footing, and the soil pressure in each vertex on the footing "σ_1, σ_2, σ_3, σ_4, σ_5, σ_6, σ_7, σ_8".

2.1 Optimal surface

The optimal surface "$S_{\min}$" of contact on the ground is (objective function) (Luévanos-Rojas *et al.* 2018a)

$$S_{\min} = (a - b_2)b_1 + bb_2 \tag{1}$$

Subject to

$$R = P_1 + P_2 \tag{2}$$

$$M_{xT} = M_{x1} + M_{x2} + P_1(y_s - L_1) + P_2(y_s - L - L_1) \tag{3}$$

$$M_{yT} = M_{y1} + M_{y2} \tag{4}$$

$$\sigma_1 = \frac{R}{S} + \frac{M_{xT}y_s}{I_x} + \frac{M_{yT}a}{2I_y} \tag{5}$$

$$\sigma_2 = \frac{R}{S} + \frac{M_{xT}y_s}{I_x} - \frac{M_{yT}a}{2I_y} \tag{6}$$

$$\sigma_3 = \frac{R}{S} + \frac{M_{xT}(y_s - b_1)}{I_x} + \frac{M_{yT}a}{2I_y} \tag{7}$$

$$\sigma_4 = \frac{R}{S} + \frac{M_{xT}(y_s - b_1)}{I_x} + \frac{M_{yT}b_2}{2I_y} \tag{8}$$

$$\sigma_5 = \frac{R}{S} + \frac{M_{xT}(y_s - b_1)}{I_x} - \frac{M_{yT}b_2}{2I_y} \tag{9}$$

$$\sigma_6 = \frac{R}{S} + \frac{M_{xT}(y_s - b_1)}{I_x} - \frac{M_{yT}a}{2I_y} \tag{10}$$

$$\sigma_7 = \frac{R}{S} - \frac{M_{xT}y_i}{I_x} + \frac{M_{yT}b_2}{2I_y} \tag{11}$$

$$\sigma_8 = \frac{R}{S} - \frac{M_{xT}y_i}{I_x} - \frac{M_{yT}b_2}{2I_y} \tag{12}$$

where R is the sum of all axial loads, M_{xT} is the sum of all the moments that result around the X axis and M_{yT} the sum of all the moments that result around the Y axis, S is area of the footing, I_x is moment of inertia around the X axis and I_y is moment of inertia around the Y axis, y_s is the distance from the center of gravity to the top end fiber of the footing, y_i is the distance from the center of gravity to the bottom

end fiber of the footing.

The geometric properties are obtained by the following equations (Luévanos-Rojas *et al.* 2018a)

$$y_s = \frac{(a-b_2){b_1}^2+b^2b_2}{2[(a-b_2)b_1+bb_2]} \tag{13}$$

$$y_i = \frac{(2b-b_1)(a-b_2)b_1+b^2b_2}{2[(a-b_2)b_1+bb_2]} \tag{14}$$

$$I_x = \frac{a^2{b_1}^4+{b_2}^2(b-b_1)^4}{12[(a-b_2)b_1+bb_2]} + \frac{ab_1b_2(b-b_1)(2b^2-bb_1+{b_1}^2)}{6[(a-b_2)b_1+bb_2]} \tag{15}$$

$$I_y = \frac{b_1a^3+(b-b_1){b_2}^3}{12} \tag{16}$$

$$0 \le \begin{Bmatrix} \sigma_1 \\ \sigma_2 \\ \sigma_3 \\ \sigma_4 \\ \sigma_5 \\ \sigma_6 \\ \sigma_7 \\ \sigma_8 \end{Bmatrix} \le \sigma_p \tag{17}$$

where: σ_p is the available permissible load capacity of the soil.

The limitations of the footing can be the following:

1.- Unrestricted sides

$$L_1 + L + \frac{c_4}{2} \le b \tag{18}$$

where: $L_1 \ge c_2/2$.

2.- A restricted side

$$\frac{c_2}{2} + L + \frac{c_4}{2} \le b \tag{19}$$

3.- Two restricted sides

$$\frac{c_2}{2} + L + \frac{c_4}{2} = b \tag{20}$$

2.2 New model for design

2.2.1 Moments and bending shear

Fig. 4 shows the critical axes according to the code (ACI 318S-14 2014) for the bending moments, and these are: For the axes parallel to the X axis are: *c'*, *d'*, *e'*, *f'*, *g'*, *h'*. For the axes parallel to the Y axis are: *a'*, *b'*.

Fig. 5 presents the critical axes according to the code (ACI 318S-14 2014) for the bending shear, and these are: For the axes parallel to the X axis are: *k'*, *l'*, *m'*, *n'*, *o'*. For the axes parallel to the Y axis are: *i'*, *j'*.

The general equations are presented below.

On the y_1-y_1 axis of $0 \le x_1 \le a/2$

$$V_{x_1} = -\int_{-w_1/2}^{w_1/2}\int_{x_1}^{a/2}\sigma_{P_1}(x,y)dxdy = \frac{P_1(2x_1-a)}{2a} + \frac{3M_{y1}(4{x_1}^2-a^2)}{2a^3} \tag{21}$$

$$M_{y_1} = \frac{P_1(2x_1-a)^2}{8a} + \frac{M_{y1}(4{x_1}^3-3a^2x_1+a^3)}{2a^3} \tag{22}$$

On the y_2 - y_2 axis of $0 \le x_2 \le b_2/2$

$$V_{x_2} = -\int_{-w_2/2}^{w_2/2}\int_{x_2}^{b_2/2}\sigma_{P_2}(x,y)dxdy = \frac{P_2(2x_2-b_2)}{2b_2} + \frac{3M_{y2}(4{x_2}^2-{b_2}^2)}{2{b_2}^3} \tag{23}$$

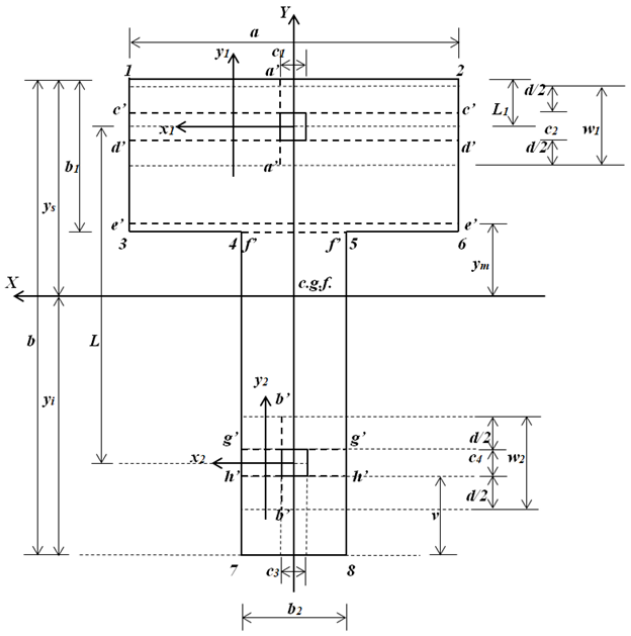

Fig. 4 Critical axes for moments according to the code ACI 318

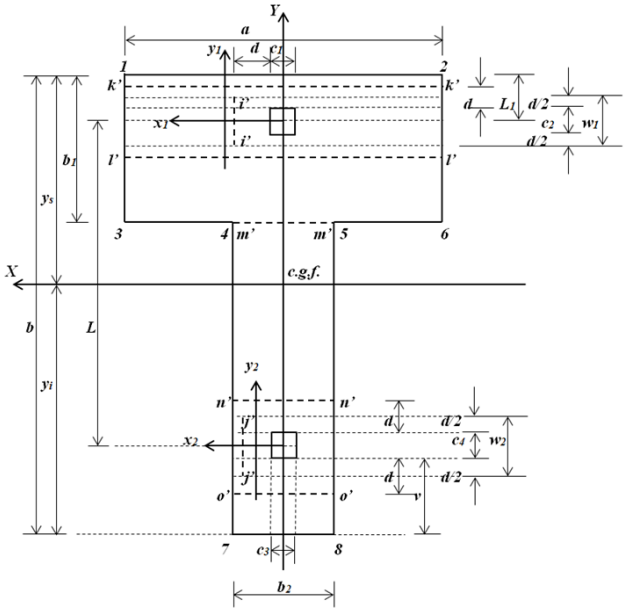

Fig. 5 Critical axes for bending shear according to the code ACI 318

where: y_m is the position of the maximum moment $M_{e'}$.

$$M_{y_2} = \frac{P_2(2x_2-b_2)^2}{8b_2} + \frac{M_{y2}(4{x_2}^3-3{b_2}^2x_2+{b_2}^3)}{2{b_2}^3} \tag{24}$$

On the x-x axis of y_s–$L_1 \le y \le y_s$

$$V_y = -\int_{y}^{y_s}\int_{-a/2}^{a/2}\sigma(x,y)dxdy = \frac{Ra(y-y_s)}{S} + \frac{M_{xT}a(y^2-{y_s}^2)}{2I_x} \tag{25}$$

$$M_x = \frac{Ra(y-y_s)^2}{2S} + \frac{M_{xT}a(y^3-3{y_s}^2y+2{y_s}^3)}{6I_x} \tag{26}$$

On the x-x axis of y_s–$b_1 \le y \le y_s$–L_1

$$V_y = P_1 - \int_y^{y_s}\int_{-a/2}^{a/2}\sigma(x,y)dxdy = P_1 + \frac{Ra(y-y_s)}{S} + \frac{M_{xT}a(y^2-{y_s}^2)}{2I_x} \quad (27)$$

$$M_x = \frac{Ra(y-y_s)^2}{2S} + \frac{M_{xT}a(y^3-3{y_s}^2y+2{y_s}^3)}{6I_x} + P_1(y-y_s+L_1) - M_{x1} \quad (28)$$

On the x-x axis of y_s–L–L_1≤y≤y_s–b_1

$$V_y = P_1 - \int_{y_s-b_1}^{y_s}\int_{-a/2}^{a/2}\sigma(x,y)dxdy - \int_y^{y_s-b_1}\int_{-b_2/2}^{b_2/2}\sigma(x,y)dxdy = P_1 - \frac{R[ab_1+b_2(y_s-y-b_1)]}{S} - \frac{M_{xT}ab_1(2y_s-b_1)}{2I_x} - \frac{M_{xT}b_2[(y_s-b_1)^2-y^2]}{2I_x} \quad (29)$$

$$M_x = -\frac{M_{xT}(a-b_2)(y_s-b_1)^2(2y_s-3y-2b_1)}{6I_x} + \frac{M_{xT}[a{y_s}^2(2y_s-3y)+b_2y^3]}{6I_x} + \frac{Rab_1(2y_s-2y-b_1)}{2S} + \frac{Rb_2(y_s-y-b_1)^2}{2S} - P_1(y_s-y-L_1) - M_{x1} \quad (30)$$

On the x-x axis of y_s–b≤y≤y_s–L–L_1

$$V_y = P_1 + P_2 - \int_{y_s-b_1}^{y_s}\int_{-a/2}^{a/2}\sigma(x,y)dxdy - \int_y^{y_s-b_1}\int_{-b_2/2}^{b_2/2}\sigma(x,y)dxdy = P_1 + P_2 - \frac{M_{xT}b_2[(y_s-b_1)^2-y^2]}{2I_x} - \frac{R[ab_1+b_2(y_s-y-b_1)]}{S} - \frac{M_{xT}ab_1(2y_s-b_1)}{2I_x} \quad (31)$$

$$M_x = -\frac{M_{xT}(a-b_2)(y_s-b_1)^2(2y_s-3y-2b_1)}{6I_x} + \frac{M_{xT}[a{y_s}^2(2y_s-3y)+b_2y^3]}{6I_x} + \frac{Rab_1(2y_s-2y-b_1)}{2S} + \frac{Rb_2(y_s-y-b_1)^2}{2S} + P_2L - R(y_s-y-L_1) - M_{x1} - M_{x2} \quad (32)$$

2.2.2 Punching shear

Fig. 6 shows the critical perimeters according to the code (ACI 318S-14 2014) for the punching shear, and these are: For the column 1 is: the perimeter formed by the points 9, 10, 11 and 12. For the column 2 is: the perimeter formed by the points 13, 14, 15 and 16.

The general equations are presented below.

For column 1

The equation to obtain the punching shear that acts on the footing is

$$V_{p1} = P_1 - \int_{y_s-L_1-c_2/2-d/2}^{y_s-L_1+c_2/2+s_1}\int_{-(c_1+d)/2}^{(c_1+d)/2}\sigma(x,y)dxdy = P_1 - \frac{R(c_1+d)(c_2+d/2+s_1)}{S} - \frac{M_{xT}(c_1+d)(y_s-L_1)(c_2+d/2+s_1)}{I_x} - \frac{M_{xT}(c_1+d)[s_1(c_2+s_1)-d/2(c_2+d/2)]}{2I_x} \quad (33)$$

where: "s_1" must meet the following relationships: if $d/2$≤L_1→s_1=$d/2$, and if $d/2$≥L_1→s_1=L_1.

For column 2

The equation to obtain the punching shear that acts on the footing is

$$V_{p2} = P_2 - \int_{y_s-L-L_1-c_4/2-s_2}^{y_s-L-L_1+c_4/2+d/2}\int_{-(c_3+d)/2}^{(c_3+d)/2}\sigma(x,y)dxdy = P_2 - \frac{R(c_3+d)(c_4+d/2+s_2)}{S} - \frac{M_{xT}(c_3+d)(y_s-L-L_1)(c_4+d/2+s_2)}{I_x} - \frac{M_{xT}(c_3+d)[d/2(c_4+d/2)-s_2(c_4+s_2)]}{2I_x} \quad (34)$$

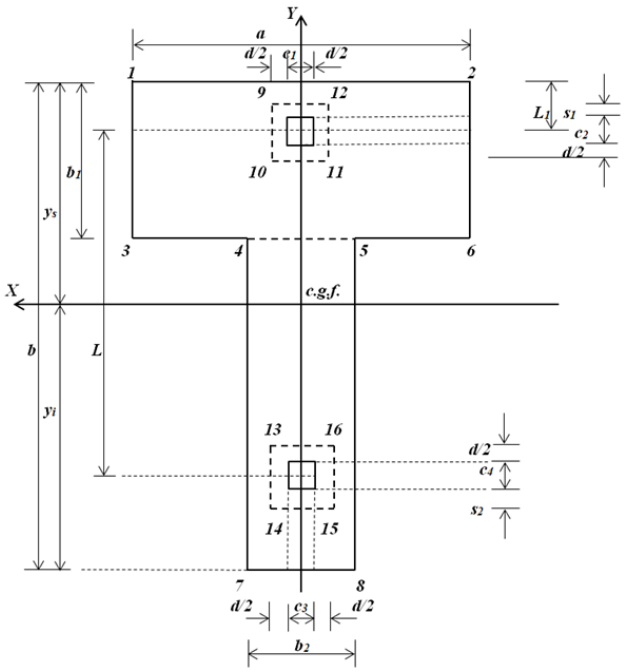

Fig. 6 Critical perimeters for punching shear according to the code ACI 318

where: "s_2" must meet the following relationships: if $d/2$≤b−L−L_1−$c_4/2$→s_2=$d/2$, and if $d/2$≥b−L−L_1−$c_4/2$→s_2=b−L−L_1−$c_4/2$.

2.3 Current model for design

The current model assumes that the position of the resultant force coincides with the center of gravity of the surface of the footing in contact with the soil in direction of the longitudinal axis. Therefore, the position of the resultant force from column 1 "y_R" is obtained

$$y_R = \frac{P_2L-(M_{x1}+M_{x2})}{P_1+P_2} \quad (35)$$

Therefore, the value "y_s" is

$$y_s = y_R + L_1 \quad (36)$$

Now, substituting "σ_p, y_s, b, b_2, R, M_{yT}" into the Eqs. (5) and (13) to obtain a and b_1.

Subsequently the stresses due to the factored loads are obtained as follows:

The uniform stress on the "X" and "Y" axes is obtained

$$\sigma_R = \frac{R}{S} \quad (37)$$

The uniform stress on the "X_1" and "Y_1" axes is

$$\sigma_{P_1} = \frac{P_1}{w_1a} \quad (38)$$

The uniform stress on the "X_2" and "Y_2" axes is

$$\sigma_{P_2} = \frac{P_2}{w_2b_2} \quad (39)$$

2.3.1 Moments

Fig. 3 shows the critical axes according to the code (ACI 318S-14 2014) for the bending moments, and these are: For

the axes parallel to the X axis are: *c'*, *d'*, *e'*, *f'*, *g'*, *h'*. For the axes parallel to the Y axis are: *a'*, *b'*.

The equations for the moments that act on each of the axes are presented below

$$M_{a'} = \frac{\sigma_{P_1} w_1 (a-c_1)^2}{8} \quad (40)$$

$$M_{b'} = \frac{\sigma_{P_2} w_2 (b_2-c_3)^2}{8} \quad (41)$$

$$M_{c'} = \frac{\sigma_R a (2L_1-c_2)^2}{8} \quad (42)$$

$$M_{d'} = \frac{\sigma_R a (2L_1+c_2)^2}{8} - \frac{P_1 c_2}{2} - M_{x1} \quad (43)$$

$$M_{f'} = \frac{\sigma_R a {b_1}^2}{2} - P_1(b_1 - L_1) - M_{x1} \quad (44)$$

If "$y_s - b_1 \leq y_m \leq y_s - L_1$"

$$y_m = y_s - \frac{P_1}{\sigma_R a} \quad (45)$$

$$M_{e'} = \frac{\sigma_R a (y_s-y_m)^2}{2} - P_1(y_s - y_m - L_1) - M_{x1} \quad (46)$$

If "$y_s - (L+L_1) \leq y_m \leq y_s - b_1$"

$$y_m = y_s + \frac{(a-b_2)b_1}{b_2} - \frac{P_1}{\sigma_p b_2} \quad (47)$$

$$M_{e'} = \sigma_R \left[ab_1\left(y_s - \frac{b_1}{2} - y_m\right) + \frac{b_2 (y_s - b_1 - y_m)^2}{2}\right] - P_1(y_s - y_m - L_1) - M_{x1} \quad (48)$$

$$M_{g'} = \sigma_R \left[ab_1\left(L + L_1 - \frac{b_1+c_4}{2}\right) + \frac{b_2}{2}\left(L + L_1 - b_1 - \frac{c_4}{2}\right)^2\right] - P_1\left(L - \frac{c_4}{2}\right) - M_{x1} \quad (49)$$

$$M_{h'} = \sigma_R \left[ab_1\left(L + L_1 - \frac{b_1-c_4}{2}\right) + \frac{b_2}{2}\left(L + L_1 - b_1 + \frac{c_4}{2}\right)^2\right] - P_1\left(L + \frac{c_4}{2}\right) - \frac{P_2 c_4}{2} - M_{x1} - M_{x2} \quad (50)$$

2.3.2 Bending shear

Fig. 4 presents the critical axes according to the code (ACI 318S-14 2014) for the bending shear, and these are: For the axes parallel to the X axis are: *k'*, *l'*, *m'*, *n'*, *o'*. For the axes parallel to the Y axis are: *i'*, *j'*.

The equations for the bending shear that act on each of the axes are presented below

$$V_i = -\frac{\sigma_{P_1} w_1 (a-c_1-2d)}{2} \quad (51)$$

$$V_j = -\frac{\sigma_{P_2} w_2 (b_2-c_3-2d)}{2} \quad (52)$$

$$V_k = -\sigma_R a\left(L_1 - \frac{c_2}{2} - d\right) \quad (53)$$

If "$y_s - b_1 \leq y_s - L_1 - c_2/2 - d$"

$$V_l = P_1 - \sigma_R a\left(L_1 + \frac{c_2}{2} + d\right) \quad (54)$$

If "$y_s - L - L_1 \leq y_s - L_1 - c_2/2 - d \leq y_s - b_1$"

$$V_l = P_1 - \sigma_R \left[ab_1 + b_2\left(L_1 - b_1 + \frac{c_2}{2} + d\right)\right] \quad (55)$$

$$V_m = P_1 - \sigma_R a b_1 \quad (56)$$

$$V_n = P_1 - \sigma_R \left[ab_1 + b_2\left(L_1 + L - b_1 - \frac{c_4}{2} - d\right)\right] \quad (57)$$

$$V_o = P_1 + P_2 - \sigma_R \left[ab_1 + b_2\left(L_1 + L - b_1 + \frac{c_4}{2} + d\right)\right] \quad (58)$$

2.3.3 Punching shear

Fig. 5 shows the critical perimeters according to the code (ACI 318S-14 2014) for the punching shear, and these are: For the column 1 is: the perimeter formed by the points 9, 10, 11 and 12. For the column 2 is: the perimeter formed by the points 13, 14, 15 and 16.

The equations for the punching shear that act on the footing are presented below

$$V_{p1} = P_1 - \sigma_R (c_1 + d)(c_2 + d/2 + s_1) \quad (59)$$

$$V_{p2} = P_2 - \sigma_R (c_3 + d)(c_4 + d/2 + s_2) \quad (60)$$

3. Verification

The equations by equilibrium in the limits of the footing can be verified for the new model as follows:

For moments around the "Y" axis: Substituting $x_1 = a/2$ into the Eq. (22) is obtained $M_{y1} = 0$. Now, substituting $x_2 = b_2/2$ into the Eq. (24) is obtained: $M_{y2} = 0$.

For moments around the "X" axis: Substituting $y = y_s$ into the Eq. (26) is obtained: $M_x = 0$. Now, substituting $y = y_s - b$ into the Eq. (32) is obtained: $M_x = 0$.

For bending shear on the "Y" axis: Substituting $x_1 = a/2$ into the Eq. (21) is obtained: $V_{x1} = 0$. Now, substituting $x_2 = b_2/2$ into the Eq. (23) is obtained: $V_{x2} = 0$.

For bending shear on the "X" axis: Substituting $y = y_s$ into the Eq. (25) is obtained: $V_y = 0$. Now, substituting $y = y_s - b$ into the Eq. (31) is obtained: $V_y = 0$.

The equations by continuity in the discontinuous sections of the footing can be verified for the new model as follows:

For moments around the "X" axis: Substituting $y = y_s - b_1$ into the Eqs. (28) and (30) is obtained the same value of M_x.

For bending shear on the "X" axis: Substituting $y = y_s - b_1$ into the Eqs. (27) and (29) is obtained the same value of V_y.

Differences of the equations in the two models:

For moments:

1.- Substituting $x_1 = c_1/2 \rightarrow c_1 = 2x_1$ and $\sigma_{P1} = P_1/w_1 a$ into Eq. (40) is obtained the Eq. (22) of the new model, but without the moment "M_{y1}".

2.- Now, substituting $x_2 = c_3/2 \rightarrow c_3 = 2x_2$ and $\sigma_{P2} = P_2/w_2 b_2$ into Eq. (41) is obtained the Eq. (24) of the new model, but the moment "M_{y2}" does not appear.

3.- Substituting $y = y_s - L_1 + c_2/2 \rightarrow c_2 = 2(y - y_s + L_1)$ and $\sigma_R = R/S$ into Eq. (42) is obtained the Eq. (26) of the new model, but without the moment "M_{xT}".

4.- Now, substituting $y = y_s - L_1 - c_2/2 \rightarrow c_2 = 2(y_s - y + L_1)$ and $\sigma_R = R/S$ into Eq. (43) is obtained the Eq. (28) of the new model, but the moment "M_{xT}" does not appear.

5.- Substituting $y = y_s - b_1 \rightarrow b_1 = y_s - y$ and $\sigma_R = R/S$ into Eq. (44) is obtained the Eq. (28) of the new model, but without the moment "M_{xT}".

6.- Now, Substituting $y=y_s-L_1-L+c_4/2\rightarrow c_4=2(y-y_s+L_1+L)$ and $\sigma_R=R/S$ into Eq. (49) is obtained the Eq. (30) of the new model, but the moment "M_{xT}" does not appear.

7.- Substituting $y=y_s-L_1-L-c_4/2\rightarrow c_4=2(y_s-y-L_1-L)$ and $\sigma_R=R/S$ into Eq. (50) is obtained the Eq. (32) of the new model, but without the moment "M_{xT}".

For bending shear:

1.- Substituting $x_1=c_1/2+d\rightarrow c_1=2(x_1-d)$ and $\sigma_{P1}=P_1/w_1a$ into Eq. (51) is obtained the Eq. (21) of the new model, but without the moment "M_{y1}".

2.- Now, substituting $x_2=c_3/2+d\rightarrow c_3=2(x_2-d)$ and $\sigma_{P2}=P_2/w_2b_2$ into Eq. (52) is obtained the Eq. (23) of the new model, but the moment "M_{y2}" does not appear.

3.- Substituting $y=y_s-L_1+c_2/2+d\rightarrow c_2=2(y-y_s+L_1-d)$ and $\sigma_R=R/S$ into Eq. (53) is obtained the Eq. (25) of the new model, but without the moment "M_{xT}".

4.- Now, substituting $y=y_s-L_1-c_2/2-d\rightarrow c_2=2(y_s-y-L_1-d)$ and $\sigma_R=R/S$ into Eq. (54) is obtained the Eq. (27) of the new model, but the moment "M_{xT}" does not appear.

5.- Now, substituting $y=y_s-L_1-c_2/2-d\rightarrow c_2=2(y_s-y-L_1-d)$ and $\sigma_R=R/S$ into Eq. (55) is obtained the Eq. (29) of the new model, but the moment "M_{xT}" does not appear.

6.- Substituting $y=y_s-b_1\rightarrow b_1=y_s-y$ and $\sigma_R=R/S$ into Eq. (56) is obtained the Eq. (27) of the new model, but without the moment "M_{xT}".

7.- Now, Substituting $y=y_s-L_1-L+c_4/2+d\rightarrow c_4=2(y-y_s+L_1+L-d)$ and $\sigma_R=R/S$ into Eq. (57) is obtained the Eq. (29) of the new model, but the moment "M_{xT}" does not appear.

8.- Substituting $y=y_s-L_1-L-c_4/2-d\rightarrow c_4=2(y_s-y-L_1-L-d)$ and $\sigma_R=R/S$ into Eq. (58) is obtained the Eq. (31) of the new model, but without the moment "M_{xT}".

For punching shear:

1.- Substituting $\sigma_R=R/S$ into Eq. (59) is obtained the Eq. (33) of the new model, but without the moment "M_{xT}".

2.- Now, substituting $\sigma_R=R/S$ into Eq. (60) is obtained the Eq. (34) of the new model, but the moment "M_{xT}" does not appear.

Therefore, the equations by equilibrium in the limits and the equations by continuity in the discontinuous sections of the footing for the new model are verified for the moments, the bending shear and the punching shear that act on the footing, and also the advantages of the new model over the current model are shown.

The comparison of the equations for the new model and the current model are shown in the Appendix (Table 1 for moments, Table 2 for bending shear and Table 3 for punching shear).

4. Numerical examples

Three numerical examples are presented below: Example 1 is for a T-shaped combined footing that supports two columns with a side restrained by a property line (Column 1 is located on the property boundary). Example 2 is for a T-shaped combined footing that supports two columns with two sides restrained (opposite sides) by two property limits (Columns 1 and 2 are located on the property boundaries). Example 3 is for a T-shaped combined footing that supports two columns with two opposite sides restrained, the column 1 is located in the center of the width of the upper flange ($b_1/2=L_1$), and column 2 is located at a distance half the width of the strip to the free end ($b_2/2=b-L_1-L$).

The thickness of the footing is obtained by means of an iterative procedure until the following three conditions are met: bending moments, bending shear, and punching shear.

The data for the three examples are: The sides of the two columns are of 40×40 cm, L=5.00 m, H (Depth of the footing)=2.0 m, P_{D1}=600 kN, P_{L1}=300 kN, M_{Dx1}=120 kN-m, M_{Lx1}=100 kN-m, M_{Dy1}=100 kN-m, M_{Ly1}=60 kN-m, P_{D2}=400 kN, P_{L2}=200 kN; M_{Dx2}=80 kN-m, M_{Lx2}=60 kN-m, M_{Dy2}=60 kN-m, M_{Ly2}=40 kN-m, f'_c (Specified compressive strength of concrete at 28 days)=28 MPa, f_y (Specified yield strength of reinforcement of steel)=420 MPa, σ_a (Permissible load capacity of the soil)=250 kN/m^2, γ_{ppz} (Density of the concrete footing)=24 kN/m^3, γ_{pps} (Density of the fill soil)=15 kN/m^3.

The loads and moments that act on soil are: P_1=900 kN, M_{x1}=220 kN-m; M_{y1}=160 kN-m, P_2=600 kN; M_{x2}=140 kN-m, M_{y2}=100 kN-m.

4.1 Example 1

Design of a T-shaped combined footing for the two models that supports two columns with a side restrained by a property line is shown below.

4.1.1 New model

The thickness that meets the bending moments, bending shear, and punching shear is of 85 cm.

Substituting the values of "σ_p=212.35 kN/m^2, P_1=900 kN, M_{x1}=220 kN-m, M_{y1}=160 kN-m, P_2=600 kN; M_{x2}=140 kN-m, M_{y2}=100 kN-m into Eqs. (1) to (17) and (19), and using the MAPLE-15 software are obtained: S_{min}=9.39 m^2, L_1=0.20 m, M_{xT}=− 273.80 kN-m, M_{yT}=260.00 kN-m, R=1500 kN, a=4.96 m, b=5.42 m, b_1=1.00 m, b_2=1.00 m, σ_1=201.32 kN/m^2, σ_2=79.09 kN/m^2, σ_3=212.35 kN/m^2, σ_4=163.55 kN/m^2, σ_5=138.92 kN/m^2, σ_6=90.12 kN/m^2, σ_7=212.35 kN/m^2, σ_8=187.72 kN/m^2.

Now, the practical dimensions of the T-shaped combined footing that supports two square columns are: a=5.00 m, b=5.45 m, b_1=1.00 m, b_2=1.00 m.

Substituting the values of "a=5.00 m, b=5.45 m, b_1=1.00 m and b_2=1.00 m" into the same MAPLE-15 software are obtained: S_{min}=9.45 m^2, L_1=0.20 m, M_{xT}=−265.20 kN-m, M_{yT}=260.00 kN-m, R=1500 kN, a=5.00 m, b=5.45 m, b_1=1.00 m, b_2=1.00 m, σ_1=200.25 kN/m^2, σ_2=79.74 kN/m^2, σ_3=210.76 kN/m^2, σ_4=162.55 kN/m^2, σ_5=138.45 kN/m^2, σ_6=90.25 kN/m^2, σ_7=209.30 kN/m^2, σ_8=185.20 kN/m^2.

Now, substituting the values of a=5.00 m, b=5.45 m, b_1=1.00 m and b_2=1.00 m into Eqs. (13) to (16) to find the geometric properties and by the Derive 6 software are obtained: y_s=1.78 m, y_i=3.67 m, I_x=25.24 m^4, I_y=10.79 m^4.

The factored loads and moments according to the code are (ACI 318S-14 2014): $P_{u1}=1.2P_{D1}+1.6P_{L1}$=1200 kN, $M_{ux1}=1.2M_{Dx1}+1.6M_{Lx1}$=304 kN-m; $M_{uy1}=1.2M_{Dy1}+1.6M_{Ly1}$=216 kN-m, $P_{u2}=1.2P_{D2}+1.6P_{L2}$=800 kN, $M_{ux2}=1.2M_{Dx2}+1.6M_{Lx2}$=192 kN-m, $M_{uy2}=1.2M_{Dy2}+1.6M_{Ly2}$=136 kN-m, R_u=2000 kN, M_{uxT}=−337.60 kN-m, M_{uyT}=352 kN-m.

4.1.2 Current model

The thickness that meets the bending moments, bending shear, and punching shear is of 85 cm.

By the Eq. (35) is found: y_R=1.76 m, and subsequently by the Eq. (36) is obtained: y_s=1.96 m.

Substituting "σ_p, y_s, b, b_2, R, M_{yT}" into the Eqs. (5) and (13) is obtained: a=3.20 m and b_1=2.19 m. Now, substituting a=3.20 m, b=5.45 m, b_1=2.19 m and b_2=1.00 m into Eqs. (1), (13) to (17) are found: S=10.28 m^2, y_s=1.96 m, y_i=3.49 m, I_x=22.21 m^4 and I_y=6.27 m^4.

Substituting the values of "σ_p=212.35 kN/m^2, R=1500 kN, M_{xT}=0 kN-m (Because the resultant force coincides with the center of gravity of the surface of the footing), M_{yT}=260 kN-m, a=3.20 m, b_2=1.00 m, S=10.28 m^2, I_y=6.27 m^4 into Eqs. (5) to (12) to verify the stresses in each vertex and these are found: σ_1=212.35 kN/m^2, σ_2=79.55 kN/m^2, σ_3=212.35 kN/m^2, σ_4=166.69 kN/m^2, σ_5=125.29 kN/m^2, σ_6=79.55 kN/m^2, σ_7=166.69 kN/m^2, σ_8=125.21 kN/m^2.

Now, the practical dimensions of the T-shaped combined footing that supports two square columns are: a=3.20 m, b=5.45 m, b_1=2.20 m, b_2=1.00 m.

Substituting the values of "a=3.20 m, b=5.45 m, b_1=2.20 m and b_2=1.00 m" into Eqs. (1), (13) to (17) are found: S=10.29 m^2, y_s=1.96 m, y_i=3.49 m, I_x=22.21 m^4 and I_y=6.28 m^4.

Now, substituting the values of "σ_p=212.35 kN/m^2, R=1500 kN, M_{xT}=0 kN-m, M_{yT}=260 kN-m, a=3.20 m, b_2=1.00 m, S=10.29 m^2, I_y=6.28 m^4 into Eqs. (5) to (12) to verify the stresses in each vertex and these are found: σ_1=212.01 kN/m^2, σ_2=79.53 kN/m^2, σ_3=212.01 kN/m^2, σ_4=166.47 kN/m^2, σ_5=125.07 kN/m^2, σ_6=79.53 kN/m^2, σ_7=166.47 kN/m^2, σ_8=125.07 kN/m^2.

The factored loads according to the code are (ACI 318S-14 2014): P_{u1}=1.2P_{D1}+1.6P_{L1}=1200 kN, P_{u2}=1.2P_{D2}+1.6P_{L2}=800 kN, R_u=2000 kN.

4.2 Example 2

Design of a T-shaped combined footing that supports two columns with two sides restrained (opposite sides) by two property limits is shown below.

4.2.1 New model

The thickness that meets the bending moments, bending shear, and punching shear is of 85 cm.

Substituting the values of "σ_p=212.35 kN/m^2, P_1=900 kN, M_{x1}=220 kN-m, M_{y1}=160 kN-m, P_2=600 kN; M_{x2}=140 kN-m, M_{y2}=100 kN-m into Eqs. (1) to (17) and (19), and using the MAPLE-15 software are obtained: S_{min}=9.40 m^2, L_1=0.20 m, M_{xT}=−273.70 kN-m, M_{yT}=260.00 kN-m, R=1500 kN, a=4.95 m, b=5.40 m, b_1=1.00 m, b_2=1.01 m, σ_1=201.25 kN/m^2, σ_2=78.55 kN/m^2, σ_3=212.35 kN/m^2, σ_4=163.52 kN/m^2, σ_5=138.47 kN/m^2, σ_6=89.64 kN/m^2, σ_7=212.35 kN/m^2, σ_8=187.30 kN/m^2.

Now, the practical dimensions of the T-shaped combined footing that supports two square columns are: a=5.00 m, b=5.40 m, b_1=1.00 m, b_2=1.05 m.

Substituting the values of "a=5.00 m, b=5.40 m, b_1=1.00 m and b_2=1.05 m" into the same MAPLE-15 software are obtained: S_{min}=9.62 m^2, L_1=0.20 m, M_{xT}=−244.99 kN-m, M_{yT}=260.00 kN-m, R=1500 kN, a=5.00 m, b=5.40 m, b_1=1.00 m, b_2=1.05 m, σ_1=198.54 kN/m^2, σ_2=78.62 kN/m^2, σ_3=208.19 kN/m^2, σ_4=160.82 kN/m^2, σ_5=135.64 kN/m^2, σ_6=88.28 kN/m^2, σ_7=203.30 kN/m^2, σ_8=178.12 kN/m^2.

Now, substituting the values of a=5.00 m, b=5.40 m, b_1=1.00 m and b_2=1.05 m into Eqs. (13) to (16) to find the geometric properties and by the Derive 6 software are obtained: y_s=1.80 m, y_i=3.60 m, I_x=25.38 m^4, I_y=10.84 m^4.

The factored loads and the moments according to the code are (ACI 318S-14 2014): P_{u1}=1.2P_{D1}+1.6P_{L1}=1200 kN, M_{ux1}=1.2M_{Dx1}+1.6M_{Lx1}=304 kN-m; M_{uy1}=1.2M_{Dy1}+1.6M_{Ly1}=216 kN-m, P_{u2}=1.2P_{D2}+1.6P_{L2}=800 kN, M_{ux2}=1.2M_{Dx2}+1.6M_{Lx2}=192 kN-m, M_{uy2}=1.2M_{Dy2}+1.6M_{Ly2}=136 kN-m, R_u=2000 kN, M_{uxT}=−310.65 kN-m, M_{uyT}=352 kN-m.

4.2.2 Current model

The thickness that meets the bending moments, bending shear, and punching shear is of 80 cm.

By the Eq. (35) is found: y_R=1.76 m, and subsequently by the Eq. (36) is obtained: y_s=1.96 m.

Substituting "σ_p, y_s, b, b_2, R, M_{yT}" into the Eqs. (5) and (13) is obtained: a=3.25 m and b_1=2.10 m. Now, substituting a=3.25 m, b=5.40 m, b_1=2.10 m and b_2=1.05 m into Eqs. (1), (13) to (17) are found: S=10.28 m^2, y_s=1.96 m, y_i=3.44 m, I_x=22.40 m^4 and I_y=6.30 m^4.

Substituting the values of "σ_p=212.80 kN/m^2, R=1500 kN, M_{xT}=0 kN-m (Because the resultant force coincides with the center of gravity of the surface of the footing), M_{yT}=260 kN-m, a=3.25 m, b_2=1.05 m, S=10.28 m^2, I_y=6.30 m^4 into Eqs. (5) to (12) to verify the stresses in each vertex and these are found: σ_1=212.80 kN/m^2, σ_2=78.95 kN/m^2, σ_3=212.80 kN/m^2, σ_4=167.52 kN/m^2, σ_5=124.22 kN/m^2, σ_6=78.95 kN/m^2, σ_7=167.52 kN/m^2, σ_8=124.22 kN/m^2.

Now, the practical dimensions of the T-shaped combined footing that supports two square columns are: a=3.25 m, b=5.40 m, b_1=2.15 m, b_2=1.05 m.

Substituting the values of "a=3.25 m, b=5.40 m, b_1=2.15 m and b_2=1.05 m" into Eqs. (1), (13) to (17) are found: S=10.40 m^2, y_s=1.96 m, y_i=3.44 m, I_x=22.41 m^4 and I_y=6.46 m^4.

Now, substituting the values of "σ_p=212.80 kN/m^2, R=1500 kN, M_{xT}=0 kN-m, M_{yT}=260 kN-m, a=3.20 m, b_2=1.00 m, S=10.29 m^2, I_y=6.28 m^4 into Eqs. (5) to (12) to verify the stresses in each vertex and these are found: σ_1=209.63 kN/m^2, σ_2=78.83 kN/m^2, σ_3=209.63 kN/m^2, σ_4=165.36 kN/m^2, σ_5=123.10 kN/m^2, σ_6=78.83 kN/m^2, σ_7=165.36 kN/m^2, σ_8=123.10 kN/m^2.

The factored loads according to the code are (ACI 318S-14 2014): P_{u1}=1.2P_{D1}+1.6P_{L1}=1200 kN, P_{u2}=1.2P_{D2}+1.6P_{L2}=800 kN, R_u=2000 kN.

4.3 Example 3

Design of a T-shaped combined footing that supports two columns with two opposite sides restrained ($b_1/2=a/2=L_1$ and $b_2/2=b–L_1–L$ is shown below.

4.3.1 New model

The thickness that meets the bending moments, bending

shear, and punching shear is of 60 cm.

Substituting the values of "σ_p=214.60 kN/m^2, P_1=900 kN, M_{x1}=220 kN-m, M_{y1}=160 kN-m, P_2=600 kN; M_{x2}=140 kN-m, M_{y2}=100 kN-m into Eqs. (1) to (17) and (19), and using the MAPLE-15 software are obtained: S_{min}=11.24 m^2, L_1=1.27 m, M_{xT}=−466.50 kN-m, M_{yT}=260.00 kN-m, R=1500 kN, a=2.54 m, b=6.83 m, b_1=2.54 m, b_2=1.11 m, σ_1=186.87 kN/m^2, σ_2=20.73 kN/m^2, σ_3=214.60 kN/m^2, σ_4=167.89 kN/m^2, σ_5=95.17 kN/m^2, σ_6=48.45 kN/m^2, σ_7=214.60 kN/m^2, σ_8=141.88 kN/m^2.

Now, the practical dimensions of the T-shaped combined footing that supports two square columns are: a=2.60 m, b=6.90 m, b_1=2.60 m, b_2=1.20 m.

Substituting the values of "a=2.60 m, b=6.90 m, b_1=2.60 m and b_2=1.20 m" into the same MAPLE-15 software are obtained: S_{min}=11.92 m^2, L_1=1.30 m, M_{xT}=−399.82 kN-m, M_{yT}=260.00 kN-m, R=1500 kN, a=2.60 m, b=6.90 m, b_1=2.60 m, b_2=1.20 m, σ_1=178.21 kN/m^2, σ_2=25.52 kN/m^2, σ_3=200.52 kN/m^2, σ_4=159.41 kN/m^2, σ_5=88.94 kN/m^2, σ_6=47.83 kN/m^2, σ_7=196.32 kN/m^2, σ_8=125.84 kN/m^2.

Now, substituting the values of a=2.60 m, b=6.90 m, b_1=2.60 m and b_2=1.20 m into Eqs. (13) to (16) to find the geometric properties and by the Derive 6 software are obtained: y_s=2.79 m, y_i=4.11 m, I_x=46.59 m^4, I_y=4.43 m^4.

The factored loads and the moments according to the code are (ACI 318S-14 2014): P_{u1}=1.2P_{D1}+1.6P_{L1}=1200 kN, M_{ux1}=1.2M$_{Dx1}$+1.6M_{Lx1}=304 kN-m; M_{uy1}=1.2M_{Dy1}+1.6M_{Ly1}=216 kN-m, P_{u2}=1.2P_{D2}+1.6P_{L2}=800 kN, M_{ux2}=1.2M_{Dx2}+1.6M_{Lx2}=192 kN-m, M_{uy2}=1.2M_{Dy2}+1.6M_{Ly2}=136 kN-m, R_u=2000 kN, M_{uxT}=−517.09 kN-m, M_{uyT}=352 kN-m.

4.3.2 Current model

The thickness that meets the bending moments, bending shear, and punching shear is of 55 cm.

By the Eq. (35) is found: y_R=1.76 m, and subsequently by the Eq. (36) is obtained: y_s=1.76+b_1/2.

Substituting "σ_p, y_s, b, b_2, R, M$_{yT}$" into the Eqs. (5) and (13) is obtained: a=2.38 m and b_2=1.34 m. Now, substituting a=2.38 m, b=6.86 m, b_1=2.38 m and b_2=1.34 m into Eqs. (1), (13) to (17) are found: S=11.67 m^2, y_s=2.95 m, y_i=3.91 m, I_x=46.99 m^4 and I_y=3.58 m^4.

Substituting the values of "σ_p=215.05 kN/m^2, R=1500 kN, M_{xT}=0 kN-m (Because the resultant force coincides with the center of gravity of the surface of the footing), M_{yT}=260 kN-m, a=2.38 m, b_2=1.34 m, S=11.67 m^2, I_y=3.58 m^4 into Eqs. (5) to (12) to verify the stresses in each vertex and these are found: σ_1=215.05 kN/m^2, σ_2=42.07 kN/m^2, σ_3=215.05 kN/m^2, σ_4=177.08 kN/m^2, σ_5=80.02 kN/m^2, σ_6=42.05 kN/m^2, σ_7=177.08 kN/m^2, σ_8=80.02 kN/m^2.

Now, the practical dimensions of the T-shaped combined footing that supports two square columns are: a=2.40 m, b=6.90 m, b_1=2.40 m, b_2=1.40 m.

Substituting the values of "a=2.40 m, b=6.90 m, b_1=2.40 m and b_2=1.40 m" into Eqs. (1), (13) to (17) are found: S=12.06 m^2, y_s=3.00 m, y_i=3.90 m, I_x=49.21 m^4 and I_y=3.79 m^4.

Now, substituting the values of "σ_p=215.05 kN/m^2, R=1500 kN, M_{xT}=0 kN-m, M_{yT}=260 kN-m, a=2.40 m, b_2=1.40 m, S=12.06 m^2, I_y=3.79 m^4 into Eqs. (5) to (12) to verify the stresses in each vertex and these are found: σ_1=206.62 kN/m^2, σ_2=42.14 kN/m^2, σ_3=206.62 kN/m^2, σ_4=172.35 kN/m^2, σ_5=76.41 kN/m^2, σ_6=42.14 kN/m^2, σ_7=172.35 kN/m^2, σ_8=76.41 kN/m^2.

The factored loads according to the code are (ACI 318S-14 2014): P_{u1}=1.2P_{D1}+1.6P_{L1}=1200 kN, P_{u2}=1.2P_{D2}+1.6P_{L2}=800 kN, R_u=2000 kN.

Table 4 Contact surface for the three examples

Concept	Example 1		Example 2		Example 3	
	NM	CM	NM	CM	NM	CM
a (m)	5.00	3.20	5.00	3.25	2.60	2.40
b (m)	5.45	5.45	5.40	5.40	6.90	6.90
b_1 (m)	1.00	2.20	1.00	2.15	2.60	2.40
b_2 (m)	1.00	1.00	1.05	1.05	1.20	1.40
S_{min} (m^2)	9.45	10.29	9.62	10.40	11.92	12.06

5. Results

Table 4 shows the contact surface for the new model "NM" and the current model "CM" of the three examples.

The results of the table 4 show the following:

1.- The value of "a" is smaller for the current model compared to the new model for the three examples.

2.- The value of "b" is same for the two models in the three examples.

3.- The value of "b_1" is smaller for the new model compared to the current model in the examples 1 and 2, and the example 3 is smaller for the current model.

4.- The value of "b_2" is same for the two models in the examples 1 and 2, and the example 3 is smaller for the new model.

5.- The value of "S_{min}" is smaller for the new model compared to the current model for the three examples.

Table 5 shows the bending moments for the two models of the three examples.

The results of the table 5 show the following:

1.- The moment greatest around the a' axis is presented in the new model for the three examples.

2.- The moment greatest around the b' axis is presented in the new model for the three examples.

3.- The moment greatest around the c' axis is presented in the new model for the example 3, and in examples 1 and 2 there is no moments because the columns are located in the property boundary.

4.- The moment greatest around the d' axis (absolute value) is presented in the current model for the three examples.

5.- The moment greatest around the e' axis (Maximum moment in absolute value) is presented in the current model for the three examples.

6.- The moment greatest around the f' axis (absolute value) is presented in the current model for the three examples.

7.- The moment greatest around the g' axis is presented in the new model for the three examples.

8.- The moment greatest around the h' axis (absolute value) is presented in the current model for the three examples.

Table 6 presents the effective depths that result from the moments for the two models of the three examples.

The results of the table 6 show the following:

Table 5 Bending moments for the three examples

Axis	Example 1				Example 2				Example 3			
	Bending moments kN-m		Analysis width cm		Bending moments kN-m		Analysis width cm		Bending moments kN-m		Analysis width cm	
	NM	CM	NM	CM	NM	CM	NM	CM	NM	CM	NM	CM
a´	729.87	367.50	78.5	78.5	729.87	374.88	78.5	76	362.50	250.00	92	87
b´	65.38	36.00	83.5	83.5	71.26	40.24	78.5	76	88.59	71.43	92	87
c´	0	0	500	320	0	0	500	325	221.56	199.00	260	240
d´	−468.17	−494.24	500	320	−468.96	−494.00	500	325	−127.68	−153.95	260	240
e´	−909.07 y_m=−0.31	−1221.65 y_m=0.63	100	100	−924.19 y_m=−0.32	−1215.99 y_m=0.04	105	105	−655.46 y_m=−0.68	−726.76 y_m=−0.45	120	140
f´	−783.37	−1198.88	100	100	−789.04	−1199.45	105	105	−577.44	−597.95	120	140
g´	58.19	34.24	100	100	53.03	30.35	105	105	112.79	25.55	120	140
h´	0.33	−17.21	100	100	0	−17.79	105	105	20.34	-71.46	120	140

where: y_m is the location of the maximum moment in absolute value

Table 6 Effective depths for the three examples

Direction	Example 1				Example 2				Example 3			
	Effective depths cm		Analysis width cm		Effective depths cm		Analysis width cm		Effective depths cm		Analysis width cm	
	NM	CM	NM	CM	NM	CM	NM	CM	NM	CM	NM	CM
X	37.76	26.79	78.5	78.5	37.76	27.50	78.5	76	24.58	20.99	92	87
Y	37.33	43.28	100	100	36.74	42.14	105	105	28.94	28.21	120	140

The proposed dimensions after several iterations are: d=77 cm, r=8 cm, t=85 cm (for the two models of the example 1); d=77 cm, r=8 cm, t=85 cm (for the new model of the example 2) and d=72 cm, r=8 cm, t=80 cm (for the current model of the example 2); d=52 cm, r=8 cm, t=60 cm (for the new model of the example 3) and d=47 cm, r=8 cm, t=55 cm (for the current model of the example 3).

Table 7 Bending shear for the three examples

Axis	Example 1						Example 2						Example 3					
	Bending shear kN				Analysis width cm		Bending shear kN				Analysis width cm		Bending shear kN				Analysis width cm	
	NM		CM		NM	CM	NM		CM		NM	CM	NM		CM		NM	CM
	V_f	$Ø_vV_f$	V_f	$Ø_vV_f$			V_f	$Ø_vV_f$	V_f	$Ø_vV_f$			V_f	$Ø_vV_f$	V_f	$Ø_vV_f$		
i´	−422	462	−236	463	78.5	78.5	−422	462	−260	418	78.5	76	−354	366	−265	313	92	87
j´	0*	492	0*	492	83.5	83.5	0*	462	0*	418	78.5	76	0*	366	−17	313	92	87
k´	0*	589	0*	1884	500	320	0*	618	0*	1789	500	325	−211	1034	−211	862	260	240
l´	193	589	472	1884	100	320	204	618	500	1789	105	325	423	1034	456	862	260	240
m´	228	589	−168	589	100	100	240	618	−144	578	105	105	178	1034	245	862	120	140
n´	−492	589	−563	589	100	100	−499	618	−574	578	105	105	−474	477	−482	503	120	140
o´	0*	588	0*	589	100	100	0*	618	0*	578	105	105	0*	477	0*	503	120	140

* The axis is located outside of the footing

1.- The effective depth greatest in direction X is presented in the new model for the three examples.

2.- The effective depth greatest in direction Y is presented in the current model for the three examples.

Table 7 shows the bending shear that acts "V_f" and the concrete resistance "$Ø_vV_f$" according to the code (ACI 318S-14 2014) for the two models of the three examples.

The results of the Table 7 show the following:

1.- The bending shear greatest that acts on *i´* axis (absolute value) is presented in the new model for the three examples.

2.- The bending shear greatest that acts on *j´* axis (absolute value) is presented in the current model for the example 3, and in examples 1 and 2 there is no bending shear because the axes are located outside of the footing.

3.- The bending shear that acts on *k´* axis is same for the two models in the example 3, and in examples 1 and 2 there is no bending shear because the axes are located outside of the footing.

4.- The bending shear greatest that acts on *l´* axis is presented in the current model for the three examples.

5.- The bending shear greatest that acts on m´ axis is presented in the new model for the examples 1 and 2, and in example 3 is presented in the current model.

6.- The bending shear greatest that acts on *n´* axis (absolute value) is presented in the current model for the three examples.

7.- The bending shear that acts on *o´* axis there is no bending shear because the axes are located outside of the footing.

Table 8 presents the punching shear that acts "V_p" and the shear that concrete resists "$Ø_vV_p$" according to the code (ACI 318S-14 2014) "$Ø_vV_f$" for both models of the three examples.

Table 8 Punching moments for the three examples

Column	Example 1				Example 2				Example 3			
	NM		CM		NM		CM		NM		CM	
	V_p	$Ø_vV_p$	V_p	$Ø_vV_p$	V_p	$Ø_vV_p$	V_p	$Ø_vV_p$	V_p	$Ø_vV_p$	V_p	$Ø_vV_p$
		4839.60		4839.60		4839.60		4360.18		4389.54		3751.85
1	1022.70	8215.41	1021.49	8215.41	1024.84	8215.41	1036.31	7225.00	1027.02	5466.53	1074.48	4519.81
		3131.51		3131.51		3131.51		2821.29		2840.29		2427.67
		4539.33		4539.33		4627.65		4244.57		4389.54		3751.85
2	550.79	8117.67	637.71	8117.67	572.95	8146.42	645.74	7187.37	625.05	5466.53	674.48	4519.81
		2937.21		2937.21		2994.36		2746.49		2840.29		2427.67

Table 9 Reinforcement steel for the three examples

Location of the steel	Type of steel	Example 1		Example 2		Example 3	
		Steel area cm^2					
		NM	CM	NM	CM	NM	CM
Direction "Y"							
Steel at the top with a width b_2	MaS	32.44	44.21	32.94	47.28	35.09	43.44
	MiS	25.67	25.67	26.95	25.20	20.80	21.93
	PS	35.42(7Ø1")	45.54(9Ø1")	35.42(7Ø1")	50.60(10Ø1")	35.42(7Ø1")	45.54(9Ø1")
Steel at the top additional to b_2, width ($a-b_2$)	TS	61.20	33.66	60.44	31.68	15.12	9.90
	PS	65.78(13Ø1")	35.42(7Ø1")	60.72(12Ø1")	35.42(7Ø1")	17.10(6Ø3/4")	11.40(4Ø1")
Steel at the bottom with a width b_2	MaS	2.00	1.18	1.83	1.12	11.46	11.37
	MiS	25.67	25.67	26.95	25.20	20.80	21.93
	PS	30.36(6Ø1")	30.36(6Ø1")	30.36(6Ø1")	25.30(5Ø1")	25.30(5Ø1")	25.30(5Ø1")
Steel at the bottom additional to b_2, width ($a-b_2$)	TS	61.20	33.66	60.44	31.68	15.12	9.90
	PS	65.78(13Ø1")	35.42(7Ø1")	60.72(12Ø1")	35.42(7Ø1")	17.10(6Ø3/4")	11.40(4Ø1")
Direction "X"							
Steel at the top with a width b	TS	83.38	83.38	82.62	77.76	74.52	68.31
	PS	86.02(17Ø1")	86.02(17Ø1")	86.02(17Ø1")	80.96(16Ø1")	75.90(15Ø1")	70.84(14Ø1")
Steel in the bottom under the column 1 with a width of w_1	MaS	26.07	12.87	26.07	14.09	19.12	14.52
	MiS	20.15	20.15	20.15	18.24	15.95	13.63
	PS	30.36(6Ø1")	20.24(4Ø1")	30.36(6Ø1")	20.24(4Ø1")	20.24(4Ø1")	15.18(3Ø1")
Steel in the bottom under the column 2 with a width of w_2	MaS	2.25	1.24	2.46	1.48	4.55	4.06
	MiS	21.43	21.43	20.15	18.24	15.95	13.63
	PS	25.30(5Ø1")	25.30(5Ø1")	20.24(4Ø1")	20.24(4Ø1")	20.24(4Ø1")	15.18(3Ø1")
Steel at the bottom additional to the columns ($b-w_1-w_2$)	TS	58.60	58.60	58.60	55.87	54.65	51.08
	PS	60.72(12Ø1")	60.72(12Ø1")	60.72(12Ø1")	60.72(12Ø1")	55.66(11Ø1")	55.66(11Ø1")

where: MaS=Main steel, MiS=Minimum steel, PS=Proposed steel, TS=Temperature steel

The results of the Table 8 show the following:

1.- The punching shear greatest that acts on the column 1 is presented in the current model for the examples 2 and 3, and in example 1 is presented in the new model.

2.- The punching shear greatest that acts on the column 2 is presented in the current model for the three examples.

Table 9 shows the reinforcement steel for the two models of the three examples.

The results of the Table 9 show the following:

1.- The steel at the top with a width "b_2" in direction Y greatest is presented in the current model for the three examples.

2.- The steel at the top additional to "b_2", width "$a-b_2$" in direction Y greatest is presented in the new model for the three examples.

3.- The steel at the bottom with a width "b_2" in direction Y greatest is presented in the new model in the example 2, and for the examples 1 and 3 is same in the two models.

4.- The steel at the bottom additional to "b_2", width "$a - b_2$" in direction Y greatest is presented in the new model for the three examples.

5.- The steel at the top with a width "b" in direction X greatest is presented in the new model in the examples 2 and 3, and for the example 1 is same in the two models.

6.- The steel in the bottom under the column 1 with a width of "w_1" in direction X greatest is presented in the new model for the three examples.

7.- The steel in the bottom under the column 2 with a width of "w_2" in direction X greatest is presented in the new model in the example 3, and for the examples 1 and 2 is same in the two models.

8.- The steel at the bottom additional to the columns "$b-w_1-w_2$" in direction X is same in the two models for the three examples.

The volume of steel by the following equation is obtained

Table 10 Volumes of steel and concrete for the three examples

Concept	Example 1		Example 2		Example 3	
	NM	CM	NM	CM	NM	CM
Volumes of steel and concrete						
V_s (cm^3)	869.12	899.89	857.72	885.32	791.84	802.84
V_c (m^3)	8.03	8.75	8.18	8.32	7.15	7.03

$$V_s = \left(A_{syTb_2} + A_{syBb_2}\right)b + \left(A_{syT(a-b_2)} + A_{syB(a-b_2)}\right)b_1 + \left[A_{sxTb}b_1/b + A_{sxBw_1} + A_{sxB(b-w_1-w_2)}(b_1 - w_1)/b\right]a + \left(A_{sxTb}(b - b_1)/b + A_{sxBw_2} + A_{sxB(b-w_1-w_2)}(b - b_1 - w_2)/b\right)b_2 \quad (61)$$

where: A_{syTb2}=Steel at the top with a width b_2 in direction "Y", A_{sBTb2}=Steel at the bottom with a width b_2 in direction "Y", $A_{syT(a-b2)}$=Steel at the top additional to b_2 ($a-b_2$) in direction "Y", $A_{syB(a-b2)}$=Steel at the bottom additional to b_2 ($a-b_2$) in direction "Y", A_{sxTb}=Steel at the top with a width b in direction "X", A_{sxBw1}=Steel in the bottom under the column 1 with a width of w_1 in direction "X", A_{sxBw2}=Steel in the bottom under the column 2 with a width of w_2 in direction "X", $A_{sxB(b-w1-w2)}$=Steel at the bottom additional to the columns ($b-w_1-w_2$) in direction "X".

The volume of concrete by the following equation is obtained

$$V_c = [(a - b_2)b_1 + bb_2]t - V_s \quad (62)$$

Table 10 shows the volume of steel "V_s", the volume of concrete "V_c" for the two models of the three examples.

The results of the Table 10 show the following:

1.- The volume of steel greatest is presented in the current model for the three examples.

2.- The volume of concrete greatest is presented in the new model for the example 3, and for the examples 1 and 2 is presented in the current model.

The parts that the current model does not consider are:

1.- The moments around of the X axis:

Substituting the loads and factored moments into Eq. (3) for the example 1 is obtained: M_{uxT}=16 kN-m.

Substituting the loads and factored moments into Eq. (3) for the example 2 is obtained: M_{uxT}=16 kN-m.

Substituting the loads and factored moments into Eq. (3) for the example 3 is obtained: M_{uxT}=96 kN-m.

2.- The moments around of the Y axis:

For the three examples are not considered: M_{uy1}=216 kN-m and M_{uy2}=136 kN-m.

6. Conclusions

The model presented in this work applies only for design of a T-shaped combined footing that supports two columns aligned on a longitudinal axis without restrictions on their sides. The considerations of this work are: the footing is rigid and the soil that supports to the footing is elastic and homogeneous, that comply with the biaxial bending, i.e., the variation of soil pressure is linear.

This paper concludes the following:

1.- The thickness for the T-shaped combined footing is governed by the bending shear on the a' axis for the new model, and for the current model on the n' axis.

2.- This model is more general and does not restrict any of its sides, because the model presented by Luévanos-Rojas *et al.* (2018) considers a side restricted or two opposite sides restricted.

3.- The new model is more suited to the real conditions with respect to the current model, because the new model considers an axial load and two moments in orthogonal directions in each column (soil pressure is linear), and the current model taking into account that the center of gravity of the footing coincides with the position of the resultant force of the loads and moments (soil pressure is uniform).

4.- The new model for design of T-shaped combined footing subjected to an axial load and two moments in orthogonal directions in each column can be used for the following considerations:

a) Without restrictions on their sides

b) One side restricted

c) Two restricted opposite sides

The next investigations can be: 1) A comparative study between the T-shaped combined footings and the trapezoidal combined footings to observe the differences. 2) Design for T-shaped combined footings supported on clay or sandy soils.

References

ACI 318S-14 (American Concrete Institute) (2014), Building Code Requirements for Structural Concrete and Commentary, Committee 318.

Agrawal, R. and Hora, M.S. (2012), "Nonlinear interaction behaviour of infilled frame-isolated footings-soil system subjected to seismic loading", *Struct. Eng. Mech.*, **44**(1), 85-107. https://doi.org/10.12989/sem.2012.44.1.085.

Alijani, M. and Bidgoli, M.R. (2018), "Agglomerated SiO_2 nanoparticles reinforced-concrete foundations based on higher order shear deformation theory: Vibration analysis", *Adv. Concrete Constr.*, **6**(6), 585-610. https://doi.org/10.12989/acc.2018.6.6.585.

Anil, Ö, Akbaş, S.O., BabagĪray, S., Gel, A.C. and Durucan, C. (2017), "Experimental and finite element analyses of footings of varying shapes on sand", *Geomech. Eng.*, **12**(2), 223-238. https://doi.org/10.12989/gae.2017.12.2.223.

Bensaid, I. and Kerboua, B. (2019), "Improvement of thermal buckling response of FG-CNT reinforced composite beams with temperature-dependent material properties resting on elastic foundations", *Adv. Aircraft Spacecraft Sci.*, **6**(3), 207-223. https://doi.org/10.12989/aas.2019.6.3.207.

Bowles, J.E. (2001), *Foundation Analysis and Design*, McGraw-Hill, New York, U.S.A.

Chen, W.R., Chen, C.S and Yu, S.Y. (2011), "Nonlinear vibration of hybrid composite plates on elastic foundations", *Struct. Eng. Mech.,* **37**(4), 367-383. https://doi.org/10.12989/sem.2011.37.4.367.

Cure, E., Sadoglu, E., Turker, E. and Uzuner, B.A. (2014), "Decrease trends of ultimate loads of eccentrically loaded model strip footings close to a slope", *Geomech. Eng.*, **6**(5), 469-485. https://doi.org/10.12989/gae.2014.6.5.469.

Dezhkam, B. and Yaghfoori, A. (2018), "Soil foundation effect on the vibration response of concrete foundations using mathematical model", *Comput. Concrete*, **22**(2), 221-225. https://doi.org/10.12989/cac.2018.22.2.221.

Dixit, M.S. and Patil K.A. (2013), "Experimental estimate of Nγ values and corresponding settlements for square footings on finite layer of sand", *Geomech. Eng.*, **5**(4), 363-377. https://doi.org/10.12989/gae.2013.5.4.363.

ErzÍn, Y. and Gul, T. O. (2013), "The use of neural networks for the prediction of the settlement of pad footings on cohesionless soils based on standard penetration test", *Geomech. Eng.*, **5**(6), 541-564. https://doi.org/10.12989/gae.2013.5.6.541.

Khatri, V.N., Debbarma, S.P., Dutta, R.K. and Mohanty, B. (2017), "Pressure-settlement behavior of square and rectangular skirted footings resting on sand", *Geomech. Eng.*, **12**(4), 689-705. https://doi.org/10.12989/gae.2017.12.4.689.

López-Chavarría, S., Luévanos-Rojas, A. and Medina-Elizondo, M. (2017), "A new mathematical model for design of square isolated footings for general case", *Int. J. Innov. Comput. I.*, **13**(4), 1149-1168.

Luévanos-Rojas, A. (2014a), "Design of isolated footings of circular form using a new model", *Struct. Eng. Mech.*, **52**(4), 767-786. http://doi.org/10.12989/sem.2014.52.4.767.

Luévanos-Rojas, A. (2014b), "Design of boundary combined footings of rectangular shape using a new model", *Dyna*, **81**(188), 199-208. http://doi.org/10.15446/dyna.v81n188.41800.

Luévanos-Rojas, A. (2015), "Design of boundary combined footings of trapezoidal form using a new model", *Struct. Eng. Mech.*, **56**(5), 745-765. https://doi.org/10.12989/sem.2015.56.5.745.

Luévanos-Rojas, A. (2016a), "A comparative study for the design of rectangular and circular isolated footings using new models", *Dyna*, **83**(196), 149-158.

Luévanos-Rojas, A. (2016b), "Un nuevo modelo para diseño de zapatas combinadas rectangulares de lindero con dos lados opuestos restringidos", *Revista Alconpat*, **6**(2), 172-187. http://doi.org/10.21041/ra.v6i2.137.

Luévanos-Rojas, A., Barquero-Cabrero, J.D., López-Chavarría, S. and Medina-Elizondo, M. (2017), "A comparative study for design of boundary combined footings of trapezoidal and rectangular forms using new models", *Couple. Syst. Mech.*, **6**(4), 417-437. https://doi.org/10.12989/csm.2017.6.4.417.

Luévanos-Rojas, A., Faudoa-Herrera, J.G., Andrade-Vallejo, R.A. and Cano-Alvarez M.A. (2013), "Design of Isolated Footings of Rectangular Form Using a New Model", *Int. J. Innov. Comput. I.*, **9**(10), 4001-4022.

Luévanos-Rojas, A., López-Chavarría, S. and Medina-Elizondo, M. (2018a), "A new model for T-shaped combined footings Part I: Optimal dimensioning", *Geomech. Eng.*, **14**(1), 51-60. https://doi.org/10.12989/gae.2018.14.1.051.

Luévanos-Rojas, A., López-Chavarría, S. and Medina-Elizondo, M. (2018b), "A new model for T-shaped combined footings Part II: Mathematical model for design", *Geomech. Eng.*, **14**(1), 61-69. https://doi.org/10.12989/gae.2018.14.1.061.

Maheshwari, P. and Khatri, S. (2012), "Influence of inclusion of geosynthetic layer on response of combined footings on stone column reinforced earth beds", *Geomech. Eng.*, **4**(4), 263-279. https://doi.org/10.12989/gae.2012.4.4.263.

Mohamed, F.M.O., Vanapalli, S.K. and Saatcioglu, M. (2013), "Generalized Schmertmann Equation for settlement estimation of shallow footings in saturated and unsaturated sands", *Geomech. Eng.*, **5**(4), 363-377. https://doi.org/10.12989/gae.2013.5.4.343.

Mohebkhah, A. (2017), "Bearing capacity of strip footings on a stone masonry trench in clay", *Geomech. Eng.*, **13**(2), 255-267. https://doi.org/10.12989/gae.2017.13.2.255.

Orbanich, C.J. and Ortega, N.F. (2013), "Analysis of elastic foundation plates with internal and perimetric stiffening beams on elastic foundations by using Finite Differences Method", *Struct. Eng. Mech.*, **45**(2), 169-182. https://doi.org/10.12989/sem.2013.45.2.169.

Orbanich, C.J., Dominguez, P.N. and Ortega, N.F. (2012), "Strenghtening and repair of concrete foundation beams whit fiber composite materials", *Mater. Struct.*, **45**(11), 1693-1704. https://doi.org/10.1617/s11527-012-9866-6.

Rad, A.B. (2012), "Static response of 2-D functionally graded circular plate with gradient thickness and elastic foundations to compound loads", *Struct. Eng. Mech.*, **44**(2), 139-161. https://doi.org/10.12989/sem.2012.44.2.139.

Shahin M.A. and Cheung E.M. (2011), "Stochastic design charts for bearing capacity of strip footings", *Geomech. Eng.*, **3**(2), 153-167. https://doi.org/10.12989/gae.2011.3.2.153.

Turedi, Y., Emirler, B., Ornek, M. and Yildiz, A. (2019), "Determination of the bearing capacity of model ring footings: Experimental and numerical investigations", *Geomech. Eng.*, **18**(1), 29-39. https://doi.org/10.12989/gae.2019.18.1.029.

Uncuoğlu, E. (2015), "The bearing capacity of square footings on a sand layer overlying clay", *Geomech. Eng.*, **9**(3), 287-311. https://doi.org/10.12989/gae.2015.9.3.287.

Yáñez-Palafox, J.A., Luévanos-Rojas, A., López-Chavarría, S. and Medina-Elizondo, M. (2019), "Modeling for the strap combined footings Part II: Mathematical model for design", *Steel Compos. Struct.*, **30**(2), 109-121. https://doi.org/10.12989/scs.2019.30.2.109.

Zhang, L., Zhao, M.H., Xiao, Y. and Ma, B.H. (2011), "Nonlinear analysis of finite beam resting on Winkler with consideration of beam-soil interface resistance effect", *Struct. Eng. Mech.*, **38**(5), 573-592. https://doi.org/10.12989/sem.2011.38.5.573.

CC

Appendix

Table 1 Differences of the equations for the moments in the two models

Concept	New model	Current model
$M_{a'}$	$\frac{P_1(a-c_1)^2}{8a}+\frac{M_{y1}(2a+c_1)(a-c_1)^2}{4a^3}$	$\frac{P_1(a-c_1)^2}{8a}$
$M_{b'}$	$\frac{P_2(b_2-c_3)^2}{8b_2}+\frac{M_{y2}(2b_2+c_3)(b_2-c_3)^2}{4{b_2}^3}$	$\frac{P_2(b_2-c_3)^2}{8b_2}$
$M_{c'}$	$\frac{Ra(2L_1-c_2)^2}{8S}+\frac{M_{xT}a\left(3y_s-L_1+\frac{c_2}{2}\right)\left(L_1-\frac{c_2}{2}\right)^2}{6I_x}$	$\frac{Ra(2L_1-c_2)^2}{8S}$
$M_{d'}$	$\frac{Ra(2L_1+c_2)^2}{8S}-\frac{P_1c_2}{2}+\frac{M_{xT}a\left(3y_s-L_1-\frac{c_2}{2}\right)\left(L_1+\frac{c_2}{2}\right)^2}{6I_x}-M_{x1}$	$\frac{Ra(2L_1+c_2)^2}{8S}-\frac{P_1c_2}{2}-M_{x1}$
$M_{e'}$	If "y_s–b_1≤y_m≤y_s–L_1"	
	$\frac{Ra(y_s-y_m)^2}{2S}+\frac{M_{xT}a({y_m}^3-3{y_s}^2y_m+2{y_s}^3)}{6I_x}-P_1(y_s-y_m-L_1)-M_{x1}$	$\frac{Ra(y_s-y_m)^2}{2S}-P_1(y_s-y_m-L_1)-M_{x1}$
	If "y_s–L–L_1≤y_m≤y_s–b_1"	
	$\frac{R[ab_1(2y_s-b_1-2y_m)+b_2(y_s-b_1-y_m)^2]}{2S}-P_1(y_s-y_m-L_1)-\frac{M_{xT}(a-b_2)(y_s-b_1)^2(2y_s-3y_m-2b_1)}{6I_x}+\frac{M_{xT}[a{y_s}^2(2y_s-3y_m)+b_2{y_m}^3]}{6I_x}-M_{x1}$	$\frac{Rab_1(2y_s-b_1-2y_m)}{2S}+\frac{Rb_2(y_s-b_1-y_m)^2}{2S}-P_1(y_s-y_m-L_1)-M_{x1}$
$M_{f'}$	$\frac{Rab_1{}^2}{2S}-P_1(b_1-L_1)-\frac{M_{xT}[a{y_s}^2(y_s-3b_1)+b_2(y_s-b_1)^3]}{6I_x}+\frac{M_{xT}(a-b_2)(y_s-b_1)^3}{6I_x}-M_{x1}$	$\frac{Rab_1{}^2}{2S}-P_1(b_1-L_1)-M_{x1}$
$M_{g'}$	$\frac{Rab_1(2L+2L_1-b_1-c_4)}{2S}+\frac{Rb_2(2L+2L_1-2b_1-c_4)^2}{8S}-\frac{P_1(2L-c_4)}{2}+\frac{M_{xT}[4a{y_s}^2(6L_1+6L-2y_s-3c_4)+b_2(2y_s-2L_1-2L+c_4)^3]}{48I_x}-\frac{M_{xT}(a-b_2)(y_s-b_1)^2(6L_1+6L-2y_s-3c_4-4b_1)}{12I_x}-M_{x1}$	$\frac{Rab_1(2L+2L_1-b_1-c_4)}{2S}+\frac{Rb_2(2L+2L_1-2b_1-c_4)^2}{8S}-\frac{P_1(2L-c_4)}{2}-M_{x1}$
$M_{h'}$	$\frac{Rab_1(2L_1+2L-b_1+c_4)}{2S}+\frac{Rb_2(2L_1+2L-2b_1+c_4)^2}{8S}-\frac{P_1(2L+c_4)}{2}-\frac{P_2c_4}{2}-\frac{M_{xT}(a-b_2)(y_s-b_1)^2(6L_1+6L-2y_s+3c_4-4b_1)}{12I_x}+\frac{M_{xT}[4a{y_s}^2(6L_1+6L-2y_s+3c_4)+b_2(2y_s-2L_1-2L-c_4)^3]}{48I_x}-M_{x1}-M_{x2}$	$\frac{Rab_1(2L_1+2L-b_1+c_4)}{2S}+\frac{Rb_2(2L_1+2L-2b_1+c_4)^2}{8S}-\frac{P_1(2L+c_4)}{2}-\frac{P_2c_4}{2}-M_{x1}-M_{x2}$

Table 2 Differences of the equations for the bending shear in the two models

Concept	New model	Current model
V_i	$-\frac{P_1(a-c_1-2d)}{2a}-\frac{3M_{y1}[a^2-(c_1+2d)^2]}{2a^3}$	$-\frac{P_1(a-c_1-2d)}{2a}$
V_j	$-\frac{P_2(b_2-c_3-2d)}{2b_2}-\frac{3M_{y2}[{b_2}^2-(c_3+2d)^2]}{2{b_2}^3}$	$-\frac{P_2(b_2-c_3-2d)}{2b_2}$
V_k	$-\frac{Ra(2L_1-c_2-2d)}{2S}-\frac{M_{xT}a(4y_s-2L_1+c_2+2d)(2L_1-c_2-2d)}{8I_x}$	$-\frac{Ra(2L_1-c_2-2d)}{2S}$
V_l	If "y_s–b_1≤y_s–L_1–$c_2/2-d$"	
	$P_1-\frac{Ra(2L_1+c_2+2d)}{2S}-\frac{M_{xT}a[4{y_s}^2-(2y_s-2L_1-c_2-2d)^2]}{8I_x}$	$P_1-\frac{Ra(2L_1+c_2+2d)}{2S}$
	If "y_s–L–L_1≤y_s–L_1–$c_2/2-d$≤y_s–b_1"	
	$P_1-\frac{R[2ab_1+b_2(2L_1-2b_1+c_2+2d)]}{2S}-\frac{M_{xT}ab_1(2y_s-b_1)}{2I_x}-\frac{M_{xT}b_2[4(y_s-b_1)^2-(2y_s-2L_1-c_2-2d)^2]}{8I_x}$	$P_1-\frac{R[2ab_1+b_2(2L_1-2b_1+c_2+2d)]}{2S}$
V_m	$P_1-\frac{Rab_1}{S}-\frac{M_{xT}ab_1(2y_s-b_1)}{2I_x}$	$P_1-\frac{Rab_1}{S}$
V_n	$P_1-\frac{R[2ab_1+b_2(2L_1+2L-2b_1-c_4-2d)]}{2S}-\frac{M_{xT}ab_1(2y_s-b_1)}{2I_x}-\frac{M_{xT}b_2[4(y_s-b_1)^2-(2y_s-2L_1-2L+c_4+2d)^2]}{8I_x}$	$P_1-\frac{R[2ab_1+b_2(2L_1+2L-2b_1-c_4-2d)]}{2S}$
V_o	$R-\frac{R[2ab_1+b_2(2L_1+2L-2b_1+c_4+2d)]}{2S}-\frac{M_{xT}ab_1(2y_s-b_1)}{2I_x}-\frac{M_{xT}b_2[4(y_s-b_1)^2-(2y_s-2L_1-2L-c_4-2d)^2]}{8I_x}$	$R-\frac{R[2ab_1+b_2(2L_1+2L-2b_1+c_4+2d)]}{2S}$

Table 3 Differences of the equations for the punching shear in the two models

Concept	New model	Current model
V_{p1}	$P_1-\frac{R(c_1+d)(2c_2+d+2s_1)}{2S}-\frac{M_{xT}(c_1+d)(y_s-L_1)(2c_2+d+2s_1)}{2I_x}-\frac{M_{xT}(c_1+d)[4s_1(c_2+s_1)-d(2c_2+d)]}{8I_x}$	$P_1-\frac{R(c_1+d)(2c_2+d+2s_1)}{2S}$
V_{p2}	$P_2-\frac{R(c_3+d)(2c_4+d+2s_2)}{2S}-\frac{M_{xT}(c_3+d)(y_s-L-L_1)(2c_4+d+2s_2)}{2I_x}-\frac{M_{xT}(c_3+d)[d(2c_4+d)-4s_2(c_4+s_2)]}{8I_x}$	$P_2-\frac{R(c_3+d)(2c_4+d+2s_2)}{2S}$